Green Hydrogen Cogeneration Through Solid-Particle Concentrated Solar Power System Integrated With Proton Exchange Membrane Stacks

Ignacio Arias[1] (iD), Felipe G. Battisti[2] (iD), José Cardemil[1] (iD), Loreto Valenzuela[3] (iD), and Rodrigo Escobar[1] (iD)

[1]Departamento de Ingeniería Mecánica y Metalúrgica, Escuela de Ingeniería Pontificia Universidad Católica de Chile, Chile

[2]Departamento de Ingeniería Mecánica, Facultad de Ingeniería, Universidad Tecnológica Metropolitana, Chile

[3]CIEMAT, Plataforma Solar de Almería, Ctra. de Senés km. 4.5, 04200, Tabernas (Almería), España

*Correspondence: Ignacio Arias, ivarias@uc.cl

Abstract. This paper presents a techno-economic analysis of third-generation (Gen3) Concentrated Solar Power (CSP) systems using solid particles and Proton Exchange Membrane (PEM) stacks for green hydrogen production. The study assesses the Levelized Cost of Hydrogen ($LCOH_2$) as a key metric. A 100 MWe CSP plant can achieve a LCOE of 55-60 $/MWh, with a Solar Multiple (SM) of 3 and Thermal Energy Storage (TES) capacity between 7 h and 16 h. Results show that a 1:1 ratio between PEM and CSP capacities is not needed to optimize hydrogen production, enabling hybrid schemes for electricity and hydrogen co-generation. However, the achieved $LCOH_2$ does not meet IEA's 2030 target of below 4 $/kg-$H_2$. Key challenges include reducing PEM costs for large-scale applications and ensuring a cost of electricity below 55 $/MWh. Addressing these issues will be crucial for the economic viability of Gen3 CSP+PEM systems in the transition to sustainable hydrogen production.

Keywords: Green Hydrogen, Solid Particles, Concentrated Solar Power, Cogeneration

1. Introduction

In the last decade, the Chilean government has promoted the country's energy transition and established public mechanisms to encourage the penetration of renewable energies in the industrial and residential sectors, compromising carbon neutrality by 2050 [1], [2]. Thus, Chile has experienced a revolution concerning electricity production. The renewable energy share of the total installed capacity has increased from 14% to 36.1% while conventional sources have decreased from 82% to 63.2% from 2016 to the beginning of 2023. Currently, 20% (i.e., 2.36 GW) of the installed renewable capacity comes from solar energy, mainly photovoltaic (PV). This is due to northern

Chile having the highest solar radiation indexes worldwide, with an average yearly total of 2600-3800 kWh/m^2-yr of Direct Normal Irradiation (DNI) and 2240-2800 kWh/m^2-yr for Global Horizontal Irradiation (GHI) [3]. However, such a massive solar potential remains underused: CSP has yet to enter the electric market with the expected force, and its integration into industrial processes is still incipient. Additionally, Chile faces two essential challenges: (a) the installation of a large capacity of variable sources, such as solar photovoltaic or wind, compromises the electrical matrix stability/flexibility, and (b) renewables alone cannot feed sectors such as heavy industry, maritime, and air transport since they require fuels that can be stored, transported, and used like fossils.

The global energy transition has clarified that other countries also face similar problems [4]. In this paradigm, hydrogen produced by renewable energies (gH$_2$) is currently proposed as a substitute vector for fossil fuels. Mainly, gH$_2$ can be stored and transported efficiently, allowing its use in different sectors, including transportation, replacing conventional sources. In addition, its use enables energy diversification and independence since relying less on imported fuels strengthens a country's energy security by reducing the inherent risks of price volatility and limited availability of non-renewable resources [5]. Using renewable sources such as solar PV, CSP, or wind to obtain hydrogen through water electrolysis does not produce greenhouse gases or atmospheric pollutants [6], [7]. Hence, it contributes to reducing the carbon footprint, improving air quality, and mitigating climate change and its adverse effects. However, the current gH$_2$ production faces different challenges associated with the scale and cost of production, storage and transportation, supply infrastructure, standards and regulations, and efficiency [8].

Solar energy may play a fundamental role in gH$_2$ production primarily because it is an inexhaustible energy source widely available worldwide, possibly leveraging hydrogen to be a sustainable clean energy solution. CSP offers specific benefits of high efficiency, thermal storage, and infrastructure [9]. The power block thermal efficiency of commercial second-generation CSP, such as central towers or parabolic troughs, can exceed 38%, thereby increasing hydrogen production from a given available solar resource. Additionally, CSP technology can integrate thermal storage systems at significantly lower costs than battery systems, allowing the storage of solar energy surplus for later use during hours without sunlight, enabling a continuous and flexible operation. Therefore, thermal storage can ensure a constant energy supply for electrolysis, resulting in high utilization factors and more stable hydrogen production.

A Gen3 CSP system can further enhance hydrogen production by using solid particles as the heat transfer medium in the receiver and a recompression supercritical carbon dioxide (s-CO$_2$) Brayton cycle [10]. Indeed, solid particles can improve the system efficiency and thermal storage capacity, allowing reaching temperatures beyond 800 °C. Meanwhile, the s-CO$_2$ as the working fluid in the Brayton cycle takes advantage of the fluid's unique thermophysical properties, enabling higher efficiencies (e.g., 50-55%) than conventional cycles [11]. Furthermore, several authors have demonstrated that solid particles CSP systems are a burgeoning field capable of achieving a low LCOE, such as 60 $/MWh [12], contributing to more efficient and cost-effective hydrogen production. However, some challenges still require careful investigation, such as operating strategies and performance optimization, which entail appropriate design and configuration of components and optimal operation of CSP and PEM systems. Therefore, continuous research and development are necessary to improve system efficiency and maximize hydrogen production, considering the specific characteristics of solid-particle CSP and PEM systems.

Furthermore, there is a need for more studies and models focusing on hydrogen production through CSP+PEM systems for specific applications, such as large-scale storage or gH_2 injection in gas pipelines. In this regard, existing studies often rely on general estimations based on stoichiometric calculations, neglecting the effects of electromotive and pressure differences, and failing to capture the impact of partial load operation. These shortcomings can lead to overestimating performance indicators such as the $LCOH_2$ and CF_{PEM}. Furthermore, to address inquiries such as is the optimal technological integration on a 1:1 scale in terms of power? Can an asymmetric relationship of nominal power capacities be established to enable a scheme that facilitates, on one hand, meeting the energy requirements of hydrogen production and, on the other hand, injecting electrical energy into the electrical grid?. Therefore, this work aims to study the techno-economic integration of Gen3 CSP based on solid particles with small and large-scale PEM systems for hydrogen and electricity production. An electrochemical model considering the system's irreversibilities simulates the PEM electrolyzer, enabling simulations of both partial-load and full-load operation. Thereby, a comprehensive analysis of the performance indicators for different subsystem scales evaluates the proposed general scheme assuming a specific application of gH_2 production with a multistage compression (MSC) system for injection into gas pipelines.

2. Methodology

2.1 System description and modeling

The analysis considers Carrera Pinto (26.96°S, 69.85°W) in the Atacama region in northern Chile. The location is 91 km from the coast and 1,915 meters above sea level (m.a.s.l), on a large desert plain between the coastal mountain range and Domeyko. Due to the above, extremely arid climatic conditions prevail in the place. This location has typical characteristics of northern Chile, i.e., low aerosol content, low cloud cover, and high levels of clear skies throughout the year. Such factors lead to high indexes of solar radiation: the average yearly totals in this location are 2500.44 kWh/m^2-yr for GHI and 3493.627 kWh/m^2-yr for DNI. The meteorological data of the place comes from an hourly typical meteorological year (TMY) obtained through Solcast [13].

Computational simulations implemented using the Openmodelica dynamic simulation software and SolarTherm library [14] assess a hybrid solid-particle Gen3 CSP+PEM system considering a central tower system with two ground-based bins. The solid-particle physics model based on Refs. [10] and [15] uses CARBO HSP 40/70 as the heat transfer medium. The Openmodelica software uses specific added models of one aperture cavity receiver (1ACR), bins, and particle lift to perform the solid-particle CSP simulations. On the other hand, PEM stack electrochemical model is based on Refs. [16], [17], [18] which has been complemented with the technical information provided in Ref. [19]. Thereby, different parametric analyzes are carried out at the system level, for 100 MW of CSP nameplate capacity, with 2 h to 20 h of TES and solar multiple (SM) of 3, integrated with small and large-scale PEM system (i.e., 0.1-100 MW_{dc}), which considers a MSC for dispatch gH_2 into gas pipelines at 80 bar [20]. For each simulated CSP system, the nominal capacity of the PEM system was obtained concerning the nominal capacity of the CSP system, defining the PEM/CSP capacity ratio ($\alpha_{PEM/CSP}$) as:

$$\alpha_{PEM/CSP} = \frac{P_{net,PEM}}{P_{net,CSP}} \qquad (1)$$
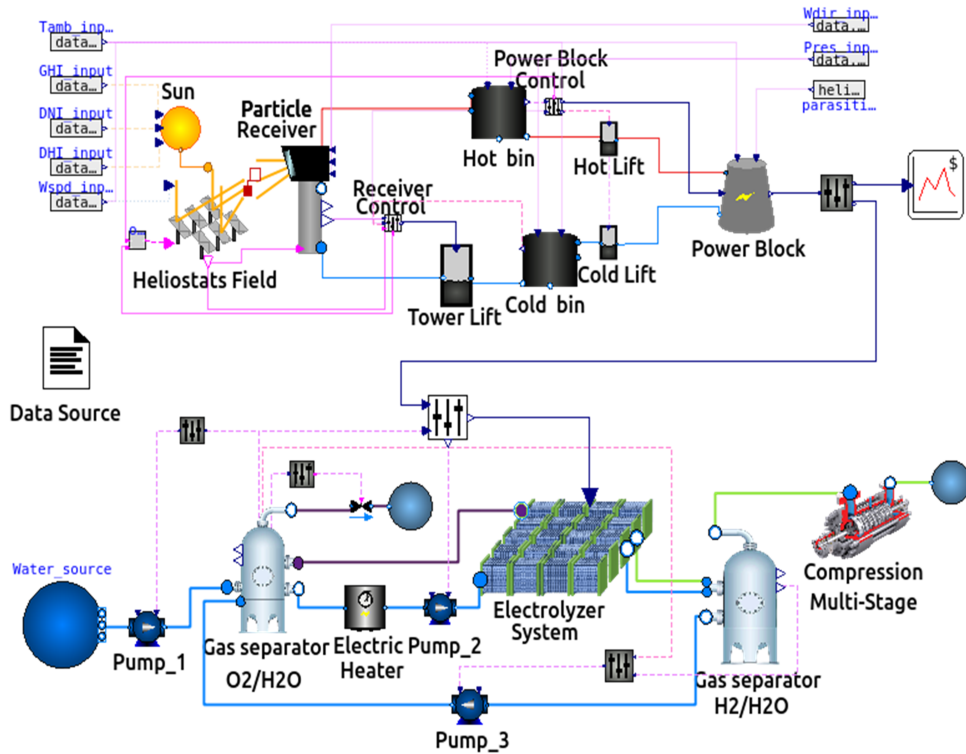
Figure 1. *System-level scheme under study within Openmodelica.*

This ratio was varied from 0.001 to 1, with steps of 0.01 to have a broader evaluation spectrum compared to the literature. Concerning the water for electrolysis, this work assumes that the feed water comes desalinated by reverse osmosis. This choice regards reverse osmosis as the most profitable way to date to obtain water from the sea for human consumption and industrial processes, and there is a vast international and national experience in its production [21]. The Techno-economic assumptions section discusses the cost of water. Thereby, Table A1 (see Appendix) summarizes the different design parameters for both the CSP and PEM systems.

The CSP's control scheme uses the models of mass flow dispatch control from SolarTherm for the power block and receiver. These consider different operational states depending on the state of charge of the hot and cold bins. Specifically, the mass flow control towards the power block has four states: off, standby, partial load, and full load. Meanwhile, the mass flow control towards the receiver has a three-state PI (proportional-integral) control that adjusts the outlet mass flow of the cold bin to reach the temperature target at the receiver outlet. Armando Fontalvo et al. [22] discusses these class models in detail. Now, the control scheme of the PEM electrolyzer uses an override control system developed based on three levels. The primary integrates a PI control scheme to regulate the current dispatch to each PEM stack, which aims to maintain operation up to the maximum current density allowed. However, if the state of charge of the oxygen/water gas separator tank is not greater than the critical value (i.e., 15%), the pumping system in the recirculation loop does not deliver flow to the electrolyzer system. This sends a feedback signal of the state of charge of the water level in the oxygen/water separator at the primary and tertiary control levels. In such a case, if the state of charge is below this critical level, the electrolyzers do not receive power, and the main water feed pump provides mass flow until reaching an acceptable level for the operation (i.e., 50%). Figure 1 depicts a detailed schematic of the system under study.

2.2 Solid-particle CSP plant model

Considering the central receiver as a 1ACR leads to selecting a polar field. The Solar Field modeling uses the steady-state Heliostats Field model from the SolarTherm library. This model computes the solar field thermal energy output ($\dot{Q}_{field}$) concentrated onto the central receiver as:

$$\dot{Q}_{field} = I_{DNI} A_{hel} N_{hel} \eta_{optical} \eta_{av} \tag{2}$$

where I_{DNI}, A_{hel}, N_{hel}, $\eta_{optical}$, and η_{av} correspond to the DNI, heliostat area, number of heliostats that compose the solar field, optical efficiency, and the availability factor, respectively. In the same way, the PSA algorithm [23] integrated in the Sun class model compute the solar angles, such as declination (δ), hour angle (ω), zenith (θ_z). The optical efficiency in each time-step is computed via interpolation from an optical efficiency lookup table (OELT) obtained through the Solstice.py wrapper by mapping sun positions on a rectangular domain – Ref. [24] discusses the solstice in detail. The OELT is interpolated through a bivariate Akima interpolation of a two-dimensional table, which uses the declination and hour angle as input elements. On the other hand, a 1-D free-falling particle receiver model based on the work of L. F. Gonzales-Portillo et al. [15] was implemented and integrated into the SolarTherm library. This model allows the discretization of the particle curtain within the receiver aperture area, considering different physical phenomena of heat transfer, such as advection, radiation, and convection, thus obtaining a better approximation of the heat absorbed during the fall of the particles. The mass, momentum, and energy balances are:

$$-\frac{d(\varphi_{pcl}(y) th_c(y) \rho_{pcl} v_{pcl}(y))}{dy} = 0 \tag{3}$$

$$-\frac{d(\varphi_{pcl} d\varphi_{pcl}(y) th_c(y) \rho_{pcl} v_{pcl}^2(y))}{dy} + \varphi_{pcl}(y) th_c(y) \rho_{pcl} g = 0 \tag{4}$$

$$\dot{Q}_{abs}(t) = \sum_{i=0}^{n} (\dot{Q}_{inc,rcv}(y_i, t) - \dot{Q}_{c,front}(y_i, t) + \dot{Q}_{gc,back}(y_i, t) - \dot{Q}_{c,back}(y_i, t) - \dot{Q}_{adv}(y_i, t)) \tag{5}$$

In Equations 1 and 2, φ_p, th_c, ρ_p, v_p, and g represent the particle volume fraction, curtain thickness, particle density, particle velocity, and gravity constant, respectively. In Equation 3, n, $\dot{Q}_{abs}$, $\dot{Q}_{inc,rcv}$, , and $\dot{Q}_{adv}$ represent the number of nodes, heat absorbed by the particle curtain, incident radiation onto the receiver, and the advection thermal losses, respectively. The terms $\dot{Q}_{c,front}$, $\dot{Q}_{c,back}$, and $\dot{Q}_{gc,back}$ represent the front and back heat flux by radiosity losses and back gain irradiance of the particle curtain, respectively. On the other hand, the thermal storage model based on the work of Gunawan et al. [10] reproduces the thermal behavior of a solid-particle sensible heat TES system. The mass and energy balances are:

$$\frac{\partial m_{pcl}}{\partial t} = \dot{m}_{pcl,in} - \dot{m}_{pcl,out} \tag{6}$$

$$m_{pcl} \frac{\partial h_{pcl}}{\partial t} + h_{pcl} \frac{\partial m_{pcl}}{\partial t} = \dot{m}_{pcl,in} h_{pcl,in} - \dot{m}_{pcl,out} h_{pcl,out} - \dot{Q}_{convection} - \dot{Q}_{radiation} \tag{7}$$

where m_{pcl}, h_{pcl}, and $\dot{m}_{pcl}$ represent the mass, enthalpy, and mass flow rate of the particles, respectively, while the subscripts in and out indicate the inlet and outlet of particles. Thus, the TES state of charge (L) comes from equating its time derivative to the ratio between the dynamic change of the volume stored (V) in each time-step and the design volume (V_{TES}) of the TES system as:

$$\frac{\partial L}{\partial t} = \frac{\frac{dV}{dt}}{V_{TES}} \tag{8}$$

The power block model uses the sCO2CycleNREL class model integrated into the SolarTherm library and based on the polynomial correlations (k_q and k_w) derived by Neises and Turchi [25] for a recompression s-CO$_2$ Brayton power cycle with dry cooling. These equations take as inputs the ambient temperature (T_{amb}), variation of the mass flow fraction at the cycle inlet (Load), and inlet temperature from the heat transfer fluid or medium to the cycle ($T_{in,PB}$). Consequently, the calculation of the power cycle's inlet heat flux ($\dot{Q}_{PB}$), gross power output (P_{gross}), and net power (P_{net}) are determined as:

$$\dot{Q}_{PB} = \dot{Q}_{PB,design} k_q(T_{in,PB}, T_{amb}, Load) \tag{9}$$

$$P_{gross} = P_{gross,design} k_w(T_{in,PB}, T_{amb}, Load) \tag{10}$$

$$P_{net} = P_{gross} - P_{base} - P_{par,loads} - P_{cooling} \tag{11}$$

where $\dot{Q}_{PB,design}$ and $P_{gross,design}$ are the heat flux to the power block and gross power at the design point, and P_{base}, $P_{par,loads}$, and $P_{cooling}$ correspond to a fixed power that represents the electrical consumption of facilities and equipment (e.g., building loads and lighting), parasitic losses, and power consumption for cooling, respectively.

2.3 Electrolyzer stack model

The electrochemical electrolyzer model based on Refs. [16], [17], [18] explains the PEM electrolyzer plant characteristics for hydrogen production, considering each cell's hydrogen and oxygen ions diffusion phenomena and the process's irreversibilities. Thereby, the electrolyzer stack voltage (V_{stack}) can be computed by:

$$\begin{aligned} V_{stack}(T, P, J, C_{O2,m}, C_{H2,m}) = N_{cell/stack} [&V_{ocv}(T, P) + V_{act,an}(J) + V_{act,cat}(J) \\ &+ V_{con,an}(T, C_{O2,m}) + V_{con,cat}(T, C_{H2,m}) + V_{ohm}(J)] \end{aligned} \tag{12}$$

where V_{ocv}, V_{act}, V_{con}, and V_{ohm} refer to the cell's open circuit, activation, concentration, and ohmic overpotentials respectively. The subscripts an and cat refer to the anode and cathode sides. Moreover, T, P, J, $C_{O2,m}$, and $C_{H2,m}$ correspond to the temperature of the electrolysis process, pressure, current density, and oxygen and hydrogen concentrations at the electrode membrane interface, respectively. The chemical species production is directly proportional to J; however, the water recovery at the anode outlet is penalized by water diffusion in the membrane, water diffusion due to the pressure difference between the anode and cathode, as well as the electro-osmotic drag effect. Thus, the molar mass of chemical species production and the water molar mass balance in each electrolyzer stack can be calculated as:

$$\dot{n}_{H2} = \dot{n}_{H2O,reac} = \frac{N_{cell/stack}J}{2F}\eta_F \qquad (13)$$

$$\dot{n}_{O2} = \frac{N_{cell/stack}J}{4F}\eta_F \qquad (14)$$

$$\dot{n}_{H2O,recup,an} = \dot{n}_{H2O,in} - \dot{n}_{H2O,reac} - \dot{n}_{mem} \qquad (15)$$

where $\dot{n}_{H2}$, $\dot{n}_{H2O,reac}$, and $\dot{n}_{O2}$ correspond to the molar mass production of hydrogen, molar mass of water reacted by stack, and molar mass production of oxygen, respectively. In Equations 12 and 13, the terms F and η_F represent the Faraday constant (96485.3365 C/mol) and the electrolyzer Faraday's efficiency, respectively. Also, in Equation 14, $\dot{n}_{H2O,in}$ and $\dot{n}_{mem}$ are the inlet water by stack and water molar mass diffusion in the membrane, respectively. Particularly, $\dot{n}_{mem}$ considers the water losses by water diffusion into the membrane by pressure difference and the electro-osmotic drag effect. Furthermore, this article does not present the calculation procedure of these parameters because Ref. [17] already discusses it thoroughly.

3. Techno-economic performance indicators

For the solid-particle CSP plant, this study assumed the cost structure of Gunawan et al. to estimate the LCOE of the CSP plant with the cost functions reported by L. F. Gonzales-Portillo et al. [12]. For techno-economic purposes, a down-selection criterion, according to U.S. Department of Energy (DOE) specifications [26], was assumed, taking a real discount rate of 4.4%, an annual inflation rate of 2.5%, 30 years of lifetime, and 0 years of construction. Anita H. Reksten et al. [27] provide the cost function used for the electrolyzer. This function allows not only to estimate the cost of the entire electrolyzer system but also to incorporate the scalability effect of the system based on the nominal power capacity of the PEM system, as well as to obtain a good estimate of the cost until the year 2030. Moreover, the operational expenditures (OPEX) of the electrolysis system depends on the evaluation scenario and the assumptions in terms of costs for the annual operational and maintenance (O&M) expenditures, electrical power, and water supplied.

On the other hand, this work assumes a fixed annual O&M expenditure cost of 2% of the capital expenditures (CAPEX) of the electrolysis system. On the other hand, this work considers a useful life of each electrolyzer stack of 90,000 h [28], which implies three replacements during the lifetime considered as the horizon of techno-economic evaluation and an electrolyzer system replacement cost equivalent to 35% of the CAPEX [29].

Additionally, with respect to the annual variable cost, the electric power and water supplied throughout the year are valorized by assuming a power purchase agreement (PPA) contract to LCOE and 3.1 \$/m^3, respectively. A. Alvez et al. [21] provide the cost of water, which includes production costs, pumping system, and piping to produce desalinated water via reverse osmosis for the Chilean territory up to 4000 m.a.s.l. Considering these aspects, Table A2 (see Appendix) summarizes the costs of the different components of the CSP and PEM electrolyzer systems. The analysis considers three techno-economic indicators such as the LCOE, LCOH$_2$, and CF$_{PEM}$, which are computed as:

$$LCOE = \frac{CAPEX_{CSP} + \sum_{i=n_{op}}^{t} \frac{OPEX_{CSP_i}}{(1+r)^i}}{\sum_{i=n_{op}}^{t} \frac{EPY_i}{(1+r)^i}} \quad (16)$$

$$LCOH_2 = \frac{CAPEX_{PEM} + \sum_{i=n_{op}}^{t} \frac{OPEX_{PEM_i}}{(1+r)^i} + \sum_{j=1}^{k} \frac{C_{rep}P_{net,PEM}}{(1+r)^{j \cdot l}}}{\sum_{i=n_{op}}^{t} \frac{HPY_i}{(1+r)^i}} \quad (17)$$

$$CF_{PEM} = \frac{HPY}{HPY_{nom}} \quad (18)$$

where EPY, HPY and HPY_{nom} correspond to the energy production per year in MWh, the hydrogen production per year in kg-yr, and the hydrogen production per year in kg-yr under nominal conditions, respectively, while r, t, k, n_{op} and l refer to the discount rate, the plant lifetime, the numbers of replacement, the year of the CSP plant's operation start and the replacement periods in years, respectively.

4. Results and discussion

Figure 2 illustrates the time-dependent operational behavior of the Solid-Particle Gen3 CSP plant of 100 MWe and SM=3 with 2 h (Figure 2a and 2c) and 10 h (Figure 2b and 2d) of TES coupled with a PEM system of 100 MW$_{dc}$ during winter (days 177 to 180) and summer (days 352 to 355), through four different variables, i.e., the net power dispatched by the CSP plant (purple surface), the PEM load state (green dash-dotted line), and the hot and cold bin states of charge (red and blue dashed lines). As shown, a large storage capacity for the CSP system allows for extending the energy production and maintaining a nominal dispatch after the sunlight hours for both winter and summer, which favor the gH$_2$ production by extending the PEM system's operational hours at full load. Also, the PEM load state fits the energy supplied by the CSP system.
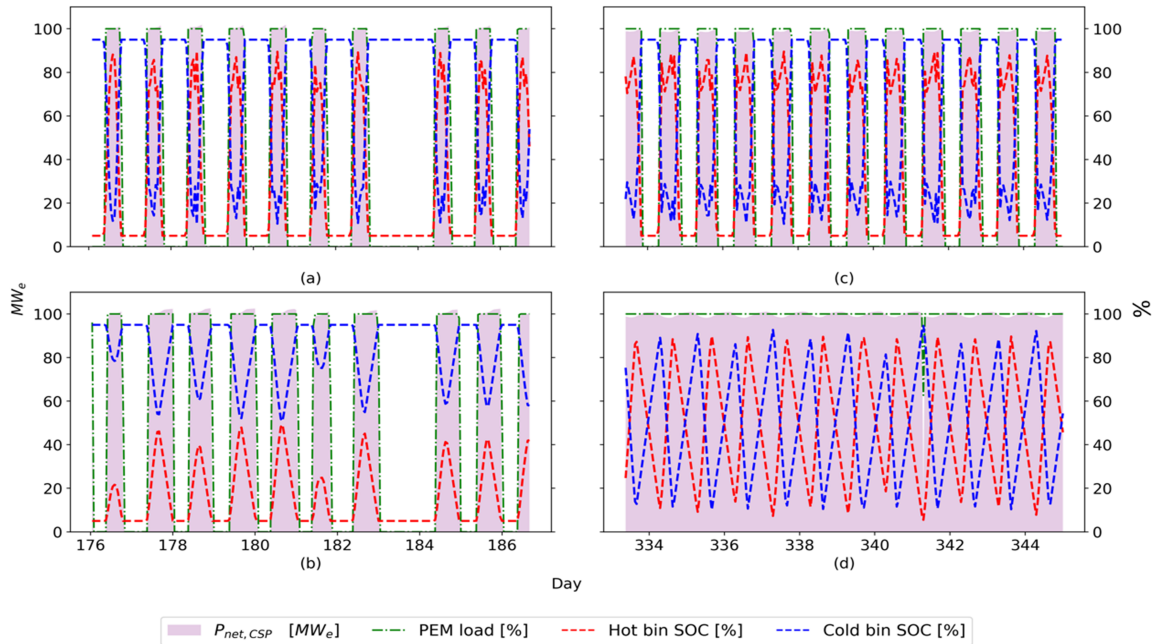

Figure 2. *Operational behavior of the Solid-Particle Gen3 CSP plant coupled with a large-scale PEM system.*

Furthermore, the PEM system can maintain its nominal operation state as long as it receives the power required from the CSP system. Therefore, regarding gH$_2$ production, it is evident that a large TES capacity will always be preferable; nevertheless, this implies increasing the LCOE, affecting the LCOH$_2$. Considering the aspects mentioned above, a parametric analysis varied the TES capacity and $\alpha_{PEM/CSP}$ from 2 to 20 h and 0.001 to 1, with steps of 0.5 h and 0.005, respectively. Figure 3 illustrates the results considering four metrics, i.e., LCOH$_2$., HPY, CF$_{PEM}$, and LCOE to identify the effect of the LCOE on LCOH$_2$, and PEM system scale from small to large scale system (from 100 to 100000 kW$_{dc}$). Indeed, Figure 3a shows that there is a clear region of minimal LCOH$_2$ between 9 h and 12 h of TES and 0.5 to 1 of $\alpha_{PEM/CSP}$. This finding is due to the combined effect of the costs of the PEM electrolyzers and energy (the latter represented by the LCOE).

Initially, transitioning from a small-scale electrolysis system to a large-scale PEM system with an installed capacity of 100 MW reduces the electrolysis system cost from over 1300$/kW$_{dc}$ to around 560 $/kW$_{dc}$ at current values (see Ref. [27]) This reduction leads to a drastic decline in LCOH$_2$ from over 8 $/kg-H$_2$ to below 6 $/kg-H$_2$ when transitioning from $\alpha_{PEM/CSP}$=0.001 to $\alpha_{PEM/CSP}$ >0.1. Furthermore, Figure 3b shows a clear dependence and the sensitivity of the LCOH$_2$ on the cost of energy supplied to the PEM system. For instance, decreasing the LCOE from 80 $/MWh to 60 $/MWh reduces the LCOH$_2$ from over 8 $/kg-H$_2$ to below 6.5 $/kg-H$_2$. Hence, it becomes evident that the LCOH$_2$ is more sensitive to the electrolysis system cost than the energy cost.
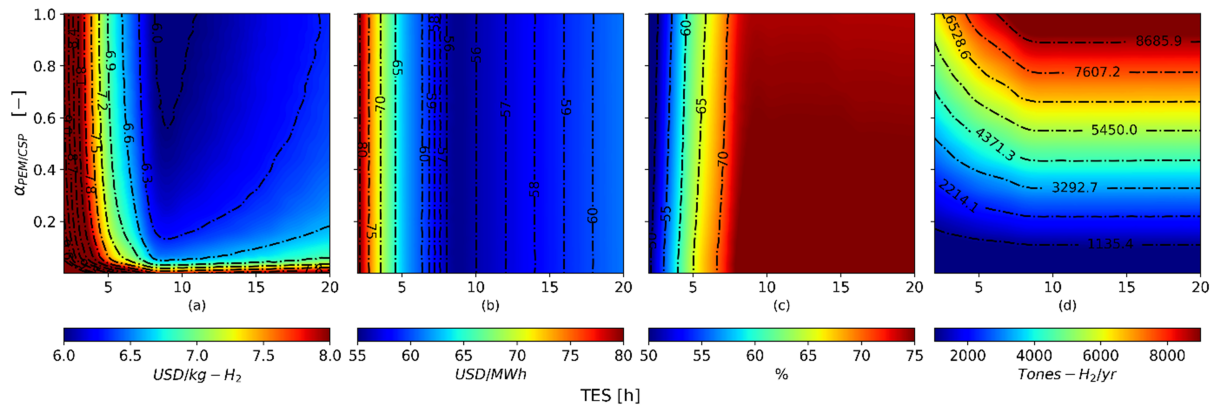

Figure 3. *Parametric analysis of the base case with a replacement cost equivalent to 35% of the PEM system's CAPEX: (a) LCOH$_2$, (b) LCOE, (c) CF$_{PEM}$, and (d) HPY*

On the other hand, Figures 3c and 3d display the PEM system's annual gH$_2$ production and CF$_{PEM}$. These figures evidence the region of highest gH$_2$ production at $\alpha_{PEM/CSP}$ >0.9 and a TES capacity of over 7 h of storage, coinciding with the region of the highest capacity factor of the PEM system (above 7 h of TES for all $\alpha_{PEM/CSP}$ values considered). However, it is unnecessary to reach a ratio of $\alpha_{PEM/CSP}$= 1 and a TES capacity of over 12 h to achieve the region with minimal LCOH$_2$ values. According to the results, it is possible to have an asymmetric proportion between the capacities of the PEM and CSP systems (i.e., 0.4< $\alpha_{PEM/CSP}$ < 0.8), allowing the latter to supply the energy requirements of the electrolysis while dispatching electrical power to the grid, which can be utilized by another industry through a Power Purchase Agreement (PPA) or sold in the spot market. This strategy enables a cogeneration scheme for electrical power consumption and gH$_2$ generation. Conversely, the LCOH$_2$ values obtained in Figure 3a, assuming the costs of the PEM system in 2023, significantly deviate from the 1.3-4.5 $/kg-H$_2$ projected by the International Energy Agency (IEA) for 2030 for

gH_2, which considers a CAPEX contraction of the PEM system of approximately 70% [30], However, it aligns with the costs of gH_2 obtained in 2021; that is, between 3-11 $/kg-$H_2$ [31].

4.1 LCOH$_2$ sensitive analysis

As previously discussed, the PEM system's CAPEX is a key factor in reducing gH_2 production costs. However, apart from the initial investment in the electrolysis system, its replacement cost over its useful life plays a crucial role in the LCOH$_2$. Different authors consider replacement costs varying significantly from each other. For instance, the DOE considers a replacement between 10-15% of the CAPEX [32], while G. Fambri et al. [29] consider 35% of the CAPEX. Hence, there is uncertainty in the industry regarding this parameter, and the present work assumes a replacement cost of 35% of the PEM system's CAPEX, i.e., a conservative value. Nevertheless, it is interesting to visualize the effect of this assumption on the LCOH$_2$.

Figure 4 illustrates the sensitivity of the LCOH$_2$ to different PEM system's replacement costs of the, specifically (a) 10%, (b) 30%, and (c) 50% of the CAPEX, considering the TES scalability and capacity, with a PEM system's cost structure referring to the years 2023 in Figures 4 a-c and 2030 in Figures 4 d-f. Considering a PEM system's cost structure for the year 2023 results in LCOH$_2$ values ranging from 4.5 to 8 $/kg-$H_2$. The comparison of these LCOH$_2$ values with the base case (see Figure 3a) evidences the replacement cost of the PEM system playing a fundamental role in the final LCOH$_2$. Indeed, reducing the replacement cost from 35% to 10% diminishes the LCOH$_2$ by approximately 25% in the region of minimum, resulting in values below 6.5 $/kg-$H_2$ for roughly the entire range under study. Similarly, increasing the replacement cost to 50% of the CAPEX increases by 15% the LCOH$_2$ compared to the base case, while the effect of reducing by 5% the replacement cost compared to the base case is somewhat negligible.

On the other hand, assuming a PEM system's cost structure referring to the year 2030 allows for obtaining LCOH$_2$ values between 4-8 $/kg-$H_2$ (see Figure 4d-f). A notable effect of the decrease in the PEM system's CAPEX and scalability considering the projected costs for 2030 is that, even with a replacement cost of 50% of the CAPEX, LCOH$_2$ values lower than those obtained in the base case for the region of minimal LCOH$_2$ values are possible. However, when observing Figure 4d, considering a replacement cost of 10% of the CAPEX with the projected installation costs for 2030 allows for achieving LCOH$_2$ values as low as 4 $/kg-$H_2$, representing a decrease of more than 30% compared to the base case and expanding the region of minimal LCOH$_2$ values even for $\alpha_{PEM/CSP}$ <0.2.

5. Conclusions

This work identified different cost-effective configurations of Gen3 CSP+PEM systems through LCOH$_2$ by adjusting the PEM system's size to the CSP system in terms of power, the TES system's capacity, the electrolysis system's cost, and its replacement cost during the established analysis horizon as its useful life. As evident from the results, Gen3 CSP technology based on solid particles can provide stable electrical power to feed PEM systems at an LCOE value between 55-60 $/MWh for a 100 MWe CSP plant with a SM=3 and a TES capacity ranging from 7 h to 16 h at the studied site. Additionally, within the range of $\alpha_{PEM/CSP}$ and the domain of TES capacity, a 1:1 relation between the installed capacities of the PEM and CSP systems is not necessary
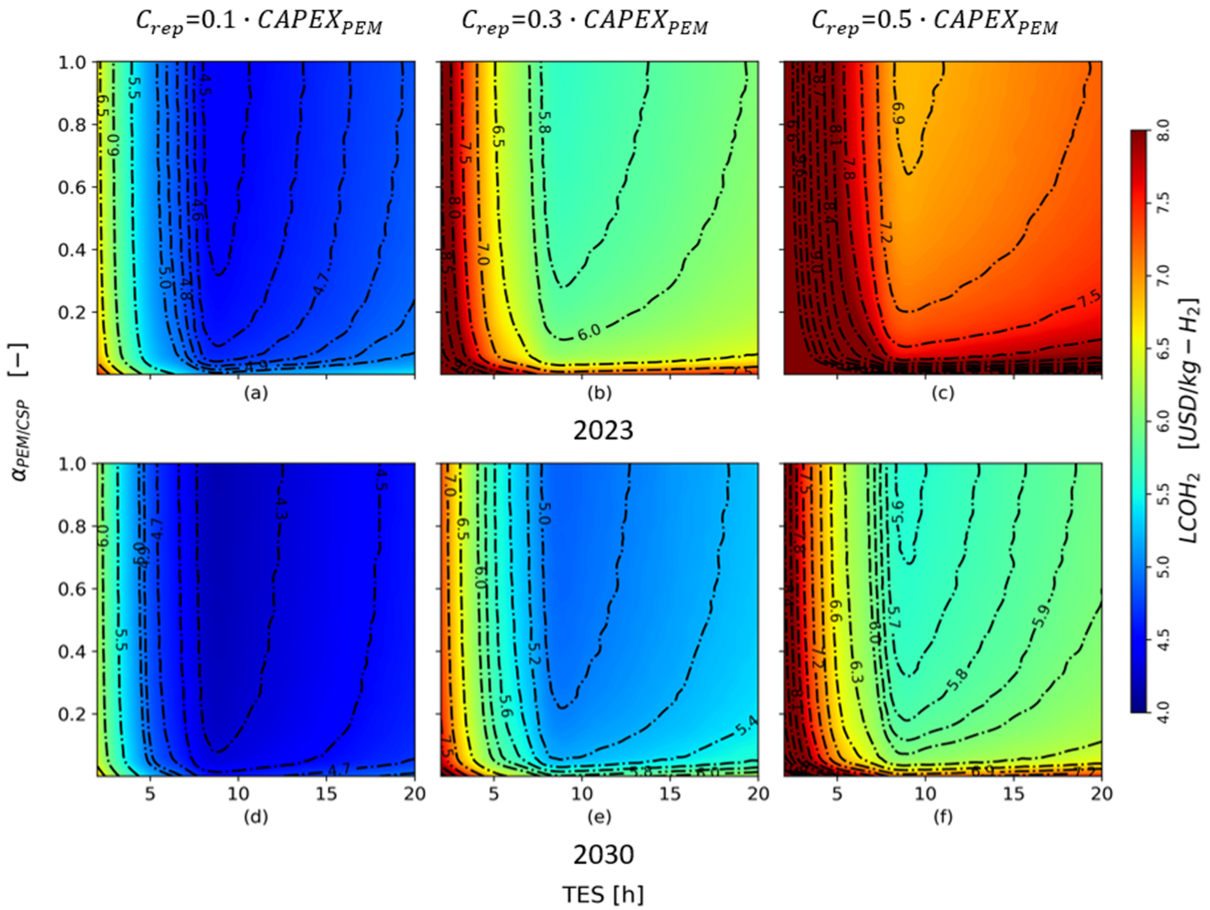
Figure 4. *Sensitivity analysis considering costs of the electrolyzation system for the years 2023 and 2030 with replacement costs at 10% (a and d), 30% (b and e), and 50% (c and f) of the PEM system's CAPEX.*

to produce gH_2 close to the technical minimum. This finding opens the possibility of hybrid schemes for co-generating electricity and gH_2 for scenarios where the PEM and CSP systems belong to the same parent company. However, such a strategy requires further analysis in terms of production and revenue perspective to minimize LCOE and $LCOH_2$ while maximizing profits.

On the other hand, the $LCOH_2$ obtained for the base case and studied scenarios of the PEM system's replacement costs show to be impossible to achieve values below 4 \$/kg-H_2 by supplying PEM systems through independent Gen3 CSP systems based on solid particles. Such a cost exceeds the expected IEA target for 2030, posing challenges in terms of the electrolysis system and energy to achieve a competitive $LCOH_2$, including:

- reducing the cost of the PEM system to below 320 \$/kW$_{dc}$ along with its replacement costs to less than 30% of the initial CAPEX for large-scale systems.
- supplying electricity to the PEM system with costs below 55 \$/MWh with a power injection that allows the system's continuous operation (i.e., achieving a CF$_{PEM}$ above 95%).

Appendix

Table A.1. *Parameter values for CSP plant and PEM electrolyzer.*

Parameter	Value	Unit	Refs.
CSP plant			
Solar Field			
DNI design point	950	W/m^2	-
Type	Polar	-	-
Heliostat width	12	m	[10]
Heliostat height	12	m	[10]
Mirror slope error	0.002	mrad	[10]
Mirror reflectivity	0.9	-	[10]
Solar Multiple	3	-	-
Receiver and TES system			
Heat transfer medium	Carbo HSP 40/70	-	[10]
Receiver view factor	0.54	-	[12], [15]
Inlet curtain velocity in the receiver	0.25	m/s	[12], [15]
Backwall thickness	0.05	m	[12], [15]
Receiver aspect ratio	1	-	[12], [15]
Receiver HTF outlet temperature at design point	800	$^\circ$C	[10], [12], [15]
Receiver coating absorptance	0.9	-	[12], [15]
Receiver coating emissivity	0.8	-	[12], [15]
Particle emissivity	0.9	-	[12], [15]
Particle volume fraction	0.6	-	[12], [15]
TES aspect ratio	1.17	-	[10]
TES hours	2 to 20	h	-
Power block			
Nameplate capacity	100	MWe	-
Power block thermal efficiency	51	%	-
PEM electrolyzer			
Membrane	Nafion 117	-	[16], [17], [19]
Platinum (Pt) loading- anode	7	g/m^2	[19]
Platinum-iridium loading- cathode	4	g/m^2	[19]
Number of cells by stack	102	-	[19]
Cells active area	680	cm^2	[19]
Max. Current density by cell at design point	17500	A/m^2	[19]
Activation energy anode electrode	57.5	kJ/mol	[19]
Activation energy cathode electrode	18	kJ/mol	[19]
Anode pre-exponential factor	10^{-7}	A/m^2	[19]
Cathode pre-exponential factor	10^{-9}	A/m^2	[19]
Anode thickness	178	μm	[16], [17], [19]
Cathode thickness	178	μm	[16], [17], [19]
Anode charge transfer coefficient	0.5	-	[16]
Cathode charge transfer coefficient	0.5	-	[16]
Membrane water content factor	23	-	-
Max. voltage by stack	240	V	[19]
Pressure electrolization	30	bar	[18]
Pressure of hydrogen at outlet compressor	80	bar	[20]
Feed water temperature at electrolyzer inlet	50	$^\circ$C	[16], [17]
Electric heater efficiency	90	%	assumed
Pump isentropic efficiency	80	%	assumed
Compressor isentropic efficiency	80	%	assumed

Table A.2. *Parameter values for techno-economic assumptions, CSP plant, and PEM electrolyzer system.*

Parameter	Value	Unit	Refs.
Transversal techno-economic assumptions			
Real discount rate	4.4	%	[10], [12]
Inflation rate	2.5	%	[10], [12]
Lifetime of the plant	30	years	[10], [12]
Time of construction	0	years	[10], [12]
State subsidies	0	$	[10], [12]
Solid-Particle CSP plant			
Risk and EPC Process Details			
Contingency (of CAPEX)	10	%	[12]
Engineering procurement and construction (EPC) (of CAPEX)	9	%	[12]
Operation cost			
Fixed O&M cost per nameplate power by year	40	$/W	[10]
Variable O&M cost per energy production by year	3	$/MWh	[10]
Balance of Plant cost per gross rated power	0.167	$/kWe	[10]
Solar field and central receiver-tower system			
Field cost per solar field aperture area	75	$/m^2	[10], [12]
Site preparation cost per solar field aperture area	10	$/m^2	[10], [12]
Land cost per	2.471	$/m^2	[10], [12]
Solid-Particle receiver cost per receiver aperture area	37400	$/m^2	[10], [12]
Tower cost	depends on the cost function	$	[12]
Lifts specific cost	58.37	$/m*(kg/s)	[12]
Thermal storage system			
Refractory material	2700	$/m^3	[10]
High-density concrete	850	$/m^3	[10]
Portland concrete	229	$/m^3	[10]
Floor filler material	150	$/m^3	[10]
Solid-Particle CARBO HSP 40/70	1	$/kg	[10]
Primary Heat Exchanger			
Heat exchanger cost per heat transfer area	6594.5	$/m^2	[10]
Particle horizontal feeder	9153	$/kg/s	[10]
sCO$_2$ piping cost	4753	$/kg/s	[10]
Power Block			
Power block cost	depends on the cost functions	$/kWe	[12]
PEM electrolyzer system			
Cost of water	3.1	$/m^3	[20]
Compressor cost	4183.6 or 3800	$/kWe or €/kWe	[33]
PEM electrolyzer plant rate cost with respect to its nominal installation capacity	depends on the cost function	$/kW	-
Fixed O&M (of CAPEX)	2	%	[33]
Contingency (of CAPEX)	5	%	[33]
Site preparation (of CAPEX)	5	%	[33]
Engineering procurement and construction (of CAPEX)	10	%	[33]
Stack lifetime	90000	h	[28]
Stacks replacement cost for base case (of CAPEX)	35 (base case)	%	[29]

Author contributions

Ignacio Arias: Conceptualization, Methodology, Software, Validation, Formal analysis, Investigation, Resources, Data curation, Writing – original draft, Writing – review & editing, Visualization, Supervision. Felipe G. Battisti: Investigation, Writing – review & editing, Visualization, Supervision. José Cardemil: Investigation, Writing – review & editing, Supervision. Loreto Valenzuela: Investigation, Writing – review & editing, Supervision. Rodrigo Escobar: Investigation, Writing – review & editing, Supervision, Resources, Writing – original draft.

Competing interests

The authors declare that they have no known competing financial interests or personal relationships that could have appeared to influence the work reported in this paper

Funding

Acknowledgement

References

[1] C. C. de Energía, "Hoja de ruta 2050 hacia una energía sustentable e inclusiva para chile," Tech. Rep., 2015, Accessed: Jul. 24, 2023. [Online]. Available: https://www.energia.gob.cl/sites/default/files/hoja_de_ruta_cc_e2050.pdf.

[2] G. de Chile, *Un hito en la historia medioambiental de chile: A partir de hoy contamos con nuestra primera ley marco de cambio climático*, Accessed: Jul. 24, 2023, 2022. [Online]. Available: https://www.gob.cl/noticias/un-hito-en-la-historia-medioambiental-de-chile-partir-de-hoy-contamos-con-nuestra-primera-ley-marco-de-cambio-climatico/.

[3] A. Castillejo-Cuberos and R. Escobar, "Understanding solar resource variability: An in-depth analysis, using chile as a case of study," *Renewable and Sustainable Energy Reviews*, vol. 120, p. 109 664, 2020, ISSN: 1364-0321. DOI: https://doi.org/10.1016/j.rser.2019.109664. [Online]. Available: https://www.sciencedirect.com/science/article/pii/S136403211930869X.

[4] T. Capurso, M. Stefanizzi, M. Torresi, and S. Camporeale, "Perspective of the role of hydrogen in the 21st century energy transition," *Energy Conversion and Management*, vol. 251, p. 114 898, 2022, ISSN: 0196-8904. DOI: https://doi.org/10.1016/j.enconman.2021.114898. [Online]. Available: https://www.sciencedirect.com/science/article/pii/S0196890421010748.

[5] A. Kovač, M. Paranos, and D. Marciuš, "Hydrogen in energy transition: A review," *International Journal of Hydrogen Energy*, vol. 46, no. 16, pp. 10 016–10 035, 2021, Hydrogen and Fuel Cells, ISSN: 0360-3199. DOI: https://doi.org/10.1016/j.ijhydene.2020.11.256. [Online]. Available: https://www.sciencedirect.com/science/article/pii/S0360319920345079.

[6] J. J. Caparrós Mancera, F. Segura Manzano, J. M. Andújar, E. López, and F. Isorna, "Sun, heat and electricity. a comprehensive study of non-pollutant alternatives to produce green hydrogen," *International Journal of Energy Research*, vol. 46, no. 13, pp. 17 999–18 028, 2022. DOI: https://doi.org/10.1002/er.8505. eprint: https://onlinelibrary.wiley.com/doi/pdf/10.1002/er.8505. [Online]. Available: https://onlinelibrary.wiley.com/doi/abs/10.1002/er.8505.

[7] L. Liu, R. Zhai, and Y. Hu, "Performance evaluation of wind-solar-hydrogen system for re-newable energy generation and green hydrogen generation and storage: Energy, exergy, economic, and enviroeconomic," *Energy*, vol. 276, p. 127 386, 2023, ISSN: 0360-5442. DOI: https://doi.org/10.1016/j.energy.2023.127386. [Online]. Available: https://www.sciencedirect.com/science/article/pii/S0360544223007806.

[8] H. Ishaq, I. Dincer, and C. Crawford, "A review on hydrogen production and utilization: Challenges and opportunities," *International Journal of Hydrogen Energy*, vol. 47, no. 62, pp. 26 238–26 264, 2022, SI: Progress in Hydrogen Production, Storage and Distribution (Ahmadi), ISSN: 0360-3199. DOI: https://doi.org/10.1016/j.ijhydene.2021.11.149. [Online]. Available: https://www.sciencedirect.com/science/article/pii/S0360319921045377.

[9] M. A. Qaisrani, J. Wei, and L. A. Khan, "Potential and transition of concentrated solar power: A case study of china," *Sustainable Energy Technologies and Assessments*, vol. 44, p. 101 052, 2021, ISSN: 2213-1388. DOI: https://doi.org/10.1016/j.seta.2021.101052. [Online]. Available: https://www.sciencedirect.com/science/article/pii/S221313882100062X.

[10] P. G. Gan, W. Ye, and P. John, "System Modelling and Optimization of a Particle-Based CSP System," *The Australian National University: Canberra, Australia*, 2021.

[11] I. Arias, J. Cardemil, E. Zarza, L. Valenzuela, and R. Escobar, "Latest developments, assessments and research trends for next generation of concentrated solar power plants using liquid heat transfer fluids," *Renewable and Sustainable Energy Reviews*, vol. 168, p. 112 844, 2022, ISSN: 1364-0321. DOI: https://doi.org/10.1016/j.rser.2022.112844. [Online]. Available: https://www.sciencedirect.com/science/article/pii/S1364032122007262.

[12] L. F. González-Portillo, K. Albrecht, and C. K. Ho, "Techno-economic optimization of csp plants with free-falling particle receivers," *Entropy*, vol. 23, no. 1, 2021, ISSN: 1099-4300. DOI: 10.3390/e23010076. [Online]. Available: https://www.mdpi.com/1099-4300/23/1/76.

[13] J. M. Bright, "Solcast: Validation of a satellite-derived solar irradiance dataset," *Solar Energy*, vol. 189, pp. 435–449, 2019, ISSN: 0038-092X. DOI: https://doi.org/10.1016/j.solener.2019.07.086. [Online]. Available: https://www.sciencedirect.com/science/article/pii/S0038092X19307571.

[14] P. Scott, A. d. l. C. Alonso, J. T. Hinkley, and J. Pye, "Solartherm: A flexible modelica-based simulator for csp systems," *AIP Conference Proceedings*, vol. 1850, no. 1, p. 160 026, Jun. 2017, ISSN: 0094-243X. DOI: 10.1063/1.4984560. eprint: https://pubs.aip.org/aip/acp/article-pdf/doi/10.1063/1.4984560/13748442/160026_1_online.pdf. [Online]. Available: https://doi.org/10.1063/1.4984560.

[15] L. F. González-Portillo, V. Soria-Alcaide, K. Albrecht, C. K. Ho, and B. Mills, "Benchmark and analysis of a particle receiver 1d model," *Solar Energy*, vol. 255, pp. 301–313, 2023, ISSN: 0038-092X. DOI: https://doi.org/10.1016/j.solener.2023.03.046. [Online]. Available: https://www.sciencedirect.com/science/article/pii/S0038092X23002062.

[16] M. Ni, M. K. Leung, and D. Y. Leung, "Energy and exergy analysis of hydrogen production by a proton exchange membrane (pem) electrolyzer plant," *Energy Conversion and Management*, vol. 49, no. 10, pp. 2748–2756, 2008, ISSN: 0196-8904. DOI: https://doi.org/10.1016/j.enconman.2008.03.018. [Online]. Available: https://www.sciencedirect.com/science/article/pii/S0196890408001210.

[17] Z. Abdin, C. Webb, and E. Gray, "Modelling and simulation of a proton exchange membrane (pem) electrolyser cell," *International Journal of Hydrogen Energy*, vol. 40, no. 39, pp. 13 243–13 257, 2015, ISSN: 0360-3199. DOI: https://doi.org/10.1016/j.ijhydene.2015.07.129. [Online]. Available: https://www.sciencedirect.com/science/article/pii/S0360319915019321.

[18] M. Schalenbach, M. Carmo, D. L. Fritz, J. Mergel, and D. Stolten, "Pressurized pem water electrolysis: Efficiency and gas crossover," *International Journal of Hydrogen Energy*, vol. 38, no. 35, pp. 14 921–14 933, 2013, ISSN: 0360-3199. DOI: https://doi.org/10.1016/j.ijhydene.2013.09.013. [Online]. Available: https://www.sciencedirect.com/science/article/pii/S0360319913022040.

[19] A. T. Mayyas, M. F. Ruth, B. S. Pivovar, G. Bender, and K. B. Wipke, "Manufacturing cost analysis for proton exchange membrane water electrolyzers," National Renewable Energy Laboratory (NREL), Golden, CO (United States), Tech. Rep., Aug. 2019. DOI: 10.2172/1557965. [Online]. Available: https://www.osti.gov/biblio/1557965.

[20] C. Tsiklios, M. Hermesmann, and T. Müller, "Hydrogen transport in large-scale transmission pipeline networks: Thermodynamic and environmental assessment of repurposed and new pipeline configurations," *Applied Energy*, vol. 327, p. 120 097, 2022, ISSN: 0306-2619. DOI: https://doi.org/10.1016/j.apenergy.2022.120097. [Online]. Available: https://www.sciencedirect.com/science/article/pii/S030626192201354X.

[21] A. Alvez, D. Aitken, D. Rivera, M. Vergara, N. McIntyre, and F. Concha, "At the crossroads: Can desalination be a suitable public policy solution to address water scarcity in chile's mining zones?" *Journal of Environmental Management*, vol. 258, p. 110 039, 2020, ISSN: 0301-4797. DOI: https://doi.org/10.1016/j.jenvman.2019.110039. [Online]. Available: https://www.sciencedirect.com/science/article/pii/S0301479719317578.

[22] A. Fontalvo et al., "System-level comparison of sodium and salt systems in support of the gen3 liquids pathway," *AIP Conference Proceedings*, vol. 2445, no. 1, p. 030 007, May 2022, ISSN: 0094-243X. DOI: 10.1063/5.0087911. eprint: https://pubs.aip.org/aip/acp/article-pdf/doi/10.1063/5.0087911/16203159/030007_1_online.pdf. [Online]. Available: https://doi.org/10.1063/5.0087911.

[23] M. J. Blanco, K. Milidonis, and A. M. Bonanos, "Updating the psa sun position algorithm," *Solar Energy*, vol. 212, pp. 339–341, 2020, ISSN: 0038-092X. DOI: https://doi.org/10.1016/j.solener.2020.10.084. [Online]. Available: https://www.sciencedirect.com/science/article/pii/S0038092X20311488.

[24] Y. Wang et al., "Verification of optical modelling of sunshape and surface slope error for concentrating solar power systems," *Solar Energy*, vol. 195, pp. 461–474, 2020, ISSN: 0038-092X. DOI: https://doi.org/10.1016/j.solener.2019.11.035. [Online]. Available: https://www.sciencedirect.com/science/article/pii/S0038092X19311338.

[25] T. Neises and C. Turchi, "Supercritical carbon dioxide power cycle design and configuration optimization to minimize levelized cost of energy of molten salt power towers operating at 650 ℃," *Solar Energy*, vol. 181, pp. 27–36, 2019, ISSN: 0038-092X. DOI: https://doi.org/10.1016/j.solener.2019.01.078. [Online]. Available: https://www.sciencedirect.com/science/article/pii/S0038092X19300908.

[26] S. Powers, "Gen 3 csp topic 1-phase 3 test facility down-selection criteria," United States Department of Energy, Office of Energy Efficiency and Renewable Energy, Tech. Rep., 2019.

[27] A. H. Reksten, M. S. Thomassen, S. Møller-Holst, and K. Sundseth, "Projecting the future cost of pem and alkaline water electrolysers; a capex model including electrolyser plant size and technology development," *International Journal of Hydrogen Energy*, vol. 47, no. 90, pp. 38 106–38 113, 2022, ISSN: 0360-3199. DOI: https://doi.org/10.1016/j.ijhydene.2022.08.306. [Online]. Available: https://www.sciencedirect.com/science/article/pii/S0360319922040253.

[28] H. Zhang and T. Yuan, "Optimization and economic evaluation of a pem electrolysis system considering its degradation in variable-power operations," *Applied Energy*, vol. 324, p. 119 760, 2022, ISSN: 0306-2619. DOI: https://doi.org/10.1016/j.apenergy.2022.119760. [Online]. Available: https://www.sciencedirect.com/science/article/pii/S030626192201042X.

[29] G. Fambri, C. Diaz-Londono, A. Mazza, M. Badami, T. Sihvonen, and R. Weiss, "Techno-economic analysis of power-to-gas plants in a gas and electricity distribution network system with high renewable energy penetration," *Applied Energy*, vol. 312, p. 118 743, 2022, ISSN: 0306-2619. DOI: https://doi.org/10.1016/j.apenergy.2022.118743. [Online]. Available: https://www.sciencedirect.com/science/article/pii/S0306261922001994.

[30] I. E. A. (IEA), "Global hydrogen review 2022," IEA, Paris, Tech. Rep., 2022, Licence: CC BY 4.0. [Online]. Available: https://www.iea.org/reports/global-hydrogen-review-2022.

[31] I. E. A. (IEA), "Energy technology perspectives 2023," IEA, Paris, Tech. Rep., 2023, License: CC BY 4.0. [Online]. Available: https://www.iea.org/reports/energy-technology-perspectives-2023.

[32] D. Peterson, J. Vickers, and D. Desantis, "Doe hydrogen and fuel cells program record: Hydrogen production cost from pem electrolysis 2019," DOE Hydrogen and Fuel Cells Program Record, Tech. Rep., 2020, [Online]. Accessed: Jul. 24, 2023, pp. 1–15. [Online]. Available: http://www.hydrogen.energy.gov/h2a_prod_studies.html.

[33] R. Hancke, T. Holm, and Ø. Ulleberg, "The case for high-pressure pem water electrolysis," *Energy Conversion and Management*, vol. 261, p. 115 642, 2022, ISSN: 0196-8904. DOI: https://doi.org/10.1016/j.enconman.2022.115642. [Online]. Available: https://www.sciencedirect.com/science/article/pii/S0196890422004381.